Langmuir

Article

pubs.acs.org/Langmuir

In-Plane Intermolecular Interaction Assisted Assembly and Modified Electronic States of Metallofullerene Gd@C_{82}

Jian Chen,[†] Zhihui Qin,*[,†] Jinbo Pan,[‡] Min Huang,[†] Shixuan Du,[‡] and Gengyu Cao[†]

[†]State Key Laboratory of Magnetic Resonance and Atomic and Molecular Physics, Wuhan Institute of Physics and Mathematics, Chinese Academy of Sciences, Wuhan 430071, P. R. China

[‡]Institute of Physics, Chinese Academy of Sciences, Beijing 100190, P. R. China

ABSTRACT: Orientational configuration and electronic states of Gd@C_{82} bonding to Cu(111) have been thoroughly investigated by low-temperature scanning tunneling microscopy/spectroscopy (LT-STM/S) and differential conductance mapping complemented by first-principles calculations. We clarify that individual Gd@C_{82} energetically adopts tilting adsorption configuration with the scanning tunneling spectroscopy (STS) states readily assigned to the C_{82} cage/Cu(111) hybrid states and the Gd/cage hybrid states, respectively. Moreover, upon assembling and sufficient thermal activation, Gd@C_{82} fullerenes are inclined to restore the energetically favored tilting orientational configuration similar to an individual one. This suggests the feasibility of high-level integration of single-Gd@C_{82} based moletronic device with the performances almost unchanged by two-dimensional arrangement. Furthermore, by rationalizing the inter-Gd@C_{82} interaction induced slight energy offset of the electronic states, we qualitatively confirm the shown electronic hybrid states as Cu(111)-, C_{82} cage- and Gd-dominant hybrid states, respectively.

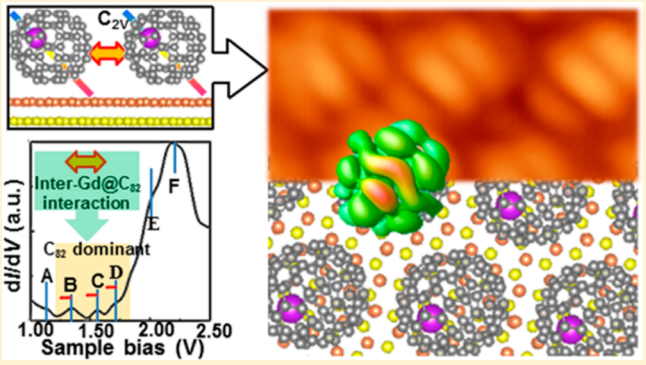

INTRODUCTION

Endohedral metallofullerenes (EMFs) have attracted remarkable attention worldwide owing to their potential application in the fields of biomedical and electronic devices, organic photovoltaics, and nanomaterial sciences, and so on.[1−5] For instance, it is reported that nanopeapod encapsulating Gd@C_{82} fullerenes modulate the bandgap of single-wall carbon nanotube,[6,7] which stimulates great interest in the unique electronic features of Gd@C_{82} for extraordinary application in spin and electronic devices. The electronic features of Gd@C_{82} relate to the exchange of electron between endohedral Gd and C_{82} cage, and to the situation of their coupling.[3,8,9] Accordingly, studies of the location of the encaged Gd in C_{82} and the coupling between them have stimulated considerable interest from both experimental and theoretical aspects, raising the controversies surrounding the geometry and electronic state of Gd@C_{82}.[8−15] More recently, the position of the encapsulated metal Gd and the reasonable electronic states of this system are clarified using spatially averaged diffraction techniques and theoretical calculations.[16,17] Most striking, however, is that while constructing the Gd@C_{82}-based moletronic device, the performances are closely associated with the particular orientation of the carbon cage with respect to the electrode substrate and the hybridization between them.[11] Moreover, studying its electronic hybrid states upon assembling on electrodes is certainly of crucial importance in seeking the feasibility of two-dimensionally integrating single-Gd@C_{82}-based moletronic devices with uniform performances.

Thus far, a few studies have been documented for Gd@C_{82} bonding to commonly used electrode materials, for example, Ag(001),[18] Cu(111),[19,20] and Cu(001),[20,21] demonstrating that the lattice spacing and symmetry of the underlying electrodes greatly affected charge transfer between the substrate and the C_{82} cage and/or between the endohedral metal and the C_{82} cage, resulting in the discrepancy in geometrical arrangement and molecular orientation of Gd@C_{82}. Additionally, since gadolinium has a large effective magnetic moment, 7.94 μB, the off-center location of Gd^{3+} ion inside C_{82} cage induces a large molecular dipole moment.[22] The resulted dipole−dipole inter-Gd@C_{82} interaction unavoidably mediates the electronic characteristics of Gd@C_{82}.

In the present study, by employing low-temperature scanning tunneling microscopy/spectroscopy (LT-STM/S) and differential conductance mapping as well as first-principles density functional theory (DFT) calculations, we study the assembly and electronic states of Gd@C_{82} on Cu(111). We choose Cu(111) as a model surface, owing to its relatively weaker interfacial interaction with Gd@C_{82} than other copper faces (e.g., Cu(001)),[20] which is the benefit of comprehensively investigating the molecular states of Gd@C_{82} and evaluating the impacts of inter-Gd@C_{82} interaction on them. Here, we clearly reveal the interfacial binding geometry and orientational

Received: August 10, 2015
Revised: October 9, 2015
Published: October 12, 2015

DOI: 10.1021/acs.langmuir.5b02965
Langmuir 2015, 31, 11438−11442

configuration of isolated Gd@C_{82} on Cu(111) and reasonably assign the scanning tunneling spectroscopy (STS) states to C_{82}-cage/Cu(111) hybrid states and Gd/cage hybrid states, respectively. We also demonstrate the temperature-activated changes in the molecular orientation of Gd@C_{82} from randomness to order. Until sufficient thermal activation at 850 K, the in-plane inter-Gd@C_{82} interaction induces Gd@C_{82} preferentially adopting tilting orientational configuration. In addition, we gain deeper insight into the origin of the STS states by evaluating the impacts of inter-Gd@C_{82} interaction on the hybrid states of Gd@C_{82}.

EXPERIMENTAL DETAILS

The experiments were performed in an ultrahigh-vacuum UNISOKU LT-STM system (base pressure <1 × 10^{-10} Torr). A single-crystal Cu(111) (MaTecK, Germany) was cleaned by repeated sputtering and annealing. Temperature was monitored by an infrared pyrometer and calibrated by a thermal couple. After thoroughly degassing at 800 K, Gd@C_{82} was sublimated at 820 K onto Cu(111) held at about 200 K with a pressure better than 8.0 × 10^{-10} Torr. All STM topographies were recorded in the constant-current mode with bias voltage V applied to the sample and were processed using WSxM.[23] The dI/dV curve was obtained by the lock-in technique with a modulation signal of 12 mV (rms) and 777 Hz, during which STM tip was kept at a fixed position.

DFT calculations were performed using the Vienna ab initio simulation package.[24] Electron−electron exchange and correlation interactions were described within the generalized gradient approximation by employing the Perdew, Burke, and Ernzerhof function.[25] In order to account for electron−ion interactions, the projector augmented wave method has been used.[26] The electronic wave functions were expanded in plane waves with a kinetic energy cutoff of 400 eV. For geometry optimization, Cu(111) was modeled with a hexagonal 5 × 5 supercell slab consisting of two atomic layers with a vacuum thickness of 10.0 Å separating the slabs. The bottom Cu layer was fixed, and the upper Cu layer of the supercell (containing Gd@C_{82}) was fully relaxed in the calculations. The structures were relaxed until the residual forces were smaller than 0.01 eV/Å. A single Γ point was used in sampling the Brillouin zone due to the numerical limitations. For accurately analyzing the interaction strength between substrate and Gd@C_{82} as well as the inter-Gd@C_{82} interaction, the van der Waals interactions were corrected by the vdW-DF2 method.[27] Spin polarization was included through all the calculations.

RESULTS AND DISCUSSION

In the very initial adsorption stage of Gd@C_{82} on Cu(111), a perspective view is shown in Figure 1, where Gd@C_{82} fullerens are observed as bright features. Gd@C_{82} fullerens bind at the step edges with a preference of locating at lower terraces as consequences of electron transfer from charge-rich Cu(111) surface to Gd@C_{82} and the Smoluchowski effect.[28] Most of Gd@C_{82} exist as individual ones, whereas some aggregate into $(Gd@C_{82})_2$ clusters along the step edge. Formation of metallofullerene cluster had been interpreted by considering the pairwise interfullerene interaction.[29] As evidenced in the inset, intramolecular details of the isolated Gd@C_{82}, for example, the one labeled by the black box, are observed as a striped pattern.

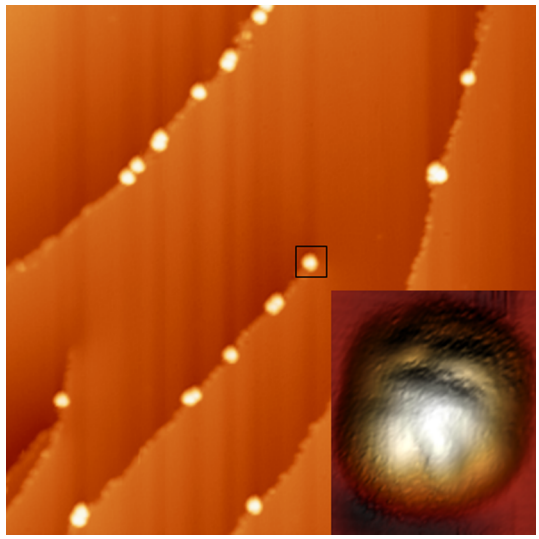

Figure 1. (a) STM image (V_{sample} = 3.00 V, I_t = 10 pA, 100 nm × 100 nm) of Gd@C_{82} initially adsorbed on Cu(111) kept at 200 K. (Inset) Intramolecular details of the isolated Gd@C_{82} labeled by black box showing stripes pattern (V_{sample} = 1.60 V, I_t = 20 pA).

A detailed energetic dependence of electronic states was checked by conducting differential conductance spectra on individual Gd@C_{82}. Because the dI/dV spectrum is sensitive to STM tip termination, the good condition of the Pt−Ir tip was verified by checking the standard spectrum (inset in Figure 2a) of the pristine Cu(111) before acquiring every dI/dV curve. The dI/dV curves obtained on isolated Gd@C_{82} are exactly consistent, demonstrating the same adsorption configuration of individual Gd@C_{82} with respect to Cu(111). As shown in Figure 2a, the dI/dV spectrum is acquired from 1.00 to 3.00 V by positioning STM tip at the center of the Gd@C_{82} labeled by the black box. The obtained curve reveals six STS states centered at 1.13 eV (**A**), 1.34 eV (**B**), 1.56 eV (**C**), 1.71 eV (**D**), 2.00 eV (**E**), and 2.24 eV (**F**), respectively. Previously, Grobis et al.[18] acquired dI/dV spectra on an isolated Gd@C_{82} residing on the edge of Ag(001). Within our detected bias range, three molecular states were revealed at 1.00, 1.32, and 1.66 eV. However, the origin of the shown states was not clearly clarified. With similar bias range as our case, Zhao et al.[20] also probed the dI/dV spectra on a single Gd@C_{82} located at Cu(111) step edge. However, only three main states were revealed at 0.80, 1.20, and 1.75 eV. Maybe the potentially different Gd@C_{82}/Cu(111) interfacial binding geometry lead to different energy positions from the molecular states obtained here. It is worth noting that our dI/dV spectrum reported here exhibits aboundant states **E** and **F**, which were never concerned in previous STS experiments.[18,20]

Thanks to the first-principles calculation, the interfacial binding geometry and the nature of the STS states can be well elucidated. The left panel in Figure 2b shows the theoretically calculated total density of states (DOS) of isolated Gd@C_{82} bound to Cu(111) with corresponding orientational configuration shown in Figure 3a. We note that the calculated orientational configuration is energetically optimized, in which the topmost copper atoms are relaxed to adapt Gd@C_{82} with a little displacement from their bulk positions. To assign the shown electronic hybrid states, we calculate the projected DOS (right panel in Figure 2b) for the bottom carbon atoms of Gd@C_{82} binding with underlying copper, the binding copper atoms

DOI: 10.1021/acs.langmuir.5b02965
Langmuir 2015, 31, 11438−11442

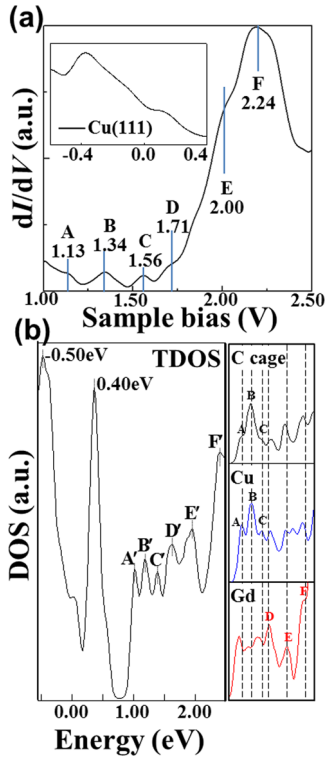

Figure 2. (a) The dI/dV curve obtained on individual Gd@C_{82} labeled by black box in Figure 1. (Inset) The dI/dV spectrum acquired on pristine Cu(111). (b) (Left panel) Theoretically calculated total DOS for energetically favored structure of isolated Gd@C_{82} on Cu(111), where peak positions are indicated by **A′**−**F′**. (Right) The projected DOS for the C atoms binding with the copper, the underlying Cu atoms and the endohedral Gd atom, respectively. The dashed lines indicate the peak positions of the dI/dV curve.

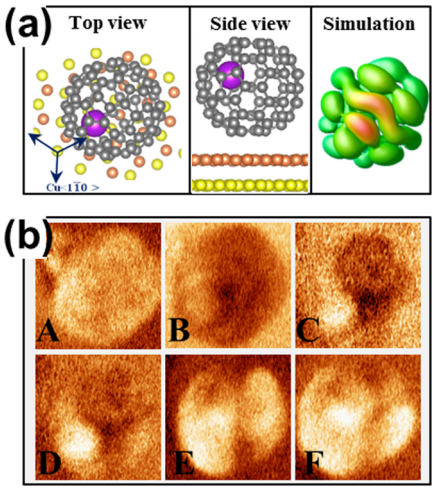

Figure 3. (a) The calculated energetically favored rotational configuration (R1) of Gd@C_{82} bonded to Cu(111) and corresponding STM simulation. The purple, gray, brown and yellow spheres indicate the Gd, C, topmost Cu, and 2nd Cu atoms, respectively. The Cu ⟨1−10⟩ vectors deduced from calculation are indicated by blue arrows. (b) dI/dV mappings at energy states **A**−**F** showing spatial distributions of the local DOS of black box labeled Gd@C_{82} in Figure 1.

and the endohedral Gd atom, respectively. Comparison of STS spectroscopy with the projected DOS clearly indicates that energy states **A**−**C** are dominated on the bottom carbon atoms and the underlying copper. They could be principally related to the hybridization of the Cu 3d electrons with the π-electrons constituting C_{82} skeletal C−C bonds.[30] The projected DOS also confirms that STS states **D**−**F** are readily relevant to Gd/cage hybrid states with majority contribution of endohedral Gd for states **E** and **F**.

STS spectra for metallofullerenes, including Gd@C_{82}, have been verified to closely relate to molecular orientation.[31] Since the energy position of the calculated molecular states **A′**−**F′** is well consistent with that of STS states **A**−**F**, it is reasonable that theoretically proposed energetically favored rotational configuration (Figure 3a, hereafter referred to R1) reflects the orientational configuration of isolated Gd@C_{82} with respect to Cu(111). Surprisingly, the side view, as depicted in the middle panel in Figure 3a, reveals that the C_{2v} axis of Gd@C_{82} tilts slightly upward from the substrate, suggesting a tilting adsorption configuration with endohedral Gd atom locating away from the surface. Previously, it is reported that Gd@C_{82} molecules tended to adopt standing-up adsorption configuration with the Gd atom pointing toward Cu(001) substrate.[21] However, as a consequence of chemisorbing to Cu(111), Ce@C_{82} were observed to have a range of orientations with endohedral Ce atom far away from the surface.[31] It seems that charge transfer between the substrate and the C_{82} cage and/or between the endohedral metal and the C_{82} cage induces different hybridization with the underlying metals, leading to different molecular orientations. The resulting potentially different M@C_{82}/substrate bonding geometry would give rise to the discrepancy in the energy position of the STS states.[18,20,31] Corresponding STM simulation (right panel in Figure 3a) shows striped structures. These characteristics fit well with available experimental observation (inset in Figure 1), once again verifying that theoretically proposed R1 orientational configuration fundamentally provides a clear picture of the interfacial binding geometry of Gd@C_{82} with respect to Cu(111).

Each molecular state has a unique spatially dependent distribution as shown in the differential conductance mapping (Figure 3b) acquired on the black box labeled Gd@C_{82} in Figure 1. Very excitingly, inside the cage one region exhibiting high electronic density (bright dot) appears at energy states **D**, **E**, and **F** and vanishes at energy states **A**−**C**. It is been inferred that the region of high spectral density within the spatial mapping of EMF molecular states was linked with the endohedral metal/cage hybrid state,[32] from which it is concluded that STS states **D**, **E**, and **F** are readily related to the Gd/cage hybrid states. The relative position of the local high electronic density inside the cage again reflects the tilting adsorption configuration of Gd@C_{82} on Cu(111).

We gain deeper insight into the nature of the STS states by evaluating the impacts of inter-Gd@C_{82} interaction on the electronic states of Gd@C_{82}. In our early study of Gd@C_{82} assemblies, we found that Gd@C_{82} adopted "lying-down" rotational configuration (Figure 2c in ref 19, hereafter referred to R2) with random azimuthal orientation.[19] It is well-known that varying the temperature could trigger an orientation transition. To verify this point, further annealing treatment was applied here. Upon annealing at 550 K, as shown in Figure 4a, Gd@C_{82} fullerens assemble into monolayer island with uniform apparent height. This is because digging the underlying copper atoms is entropically favored under every Gd@C_{82} at 550 K. Gd@C_{82} are observed as striped structure with varied direction, implying the discrepancy in the interfacial binding geometry of

DOI: 10.1021/acs.langmuir.5b02965
Langmuir 2015, 31, 11438−11442

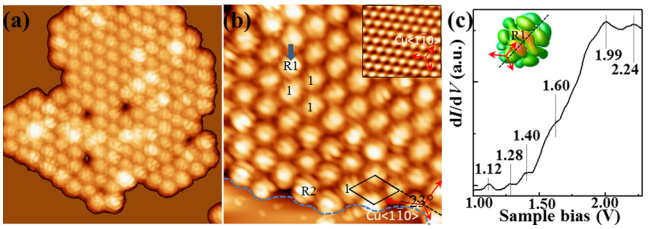

Figure 4. STM image (V_{sample} = 2.00 V, I_t = 50 pA, 15 nm × 15 nm) of a Gd@C_{82} molecular island forming upon annealing at 550 K. (b) STM image (V_{sample} = 0.60 V, I_t = 40 pA, 10 nm × 10 nm) of a close-packed ($\sqrt{19} \times \sqrt{19}$) R23.4° Gd@$C_{82}$ island following annealing at 850 K. For clarity, the unit cell is indicated by the black rhombus. And the step edge of the two monatomic terrace is indicated by dashed line. The Cu ⟨1−10⟩ vectors indicated by red arrows are deduced from the atomic resolution STM image (Inset) of the pristine Cu(111) adjacent to the Gd@C_{82} island. (c) The dI/dV curve detected on the center of the arrow indicated Gd@C_{82} with R1 orientation, where peak positions are denoted by values.

Gd@C_{82}/Cu(111), which demonstrates that Gd@C_{82} fullerens reconstruct the underlying Cu(111) lattice in varying degrees at 550 K.

Further annealing at 850 K encourages Gd@C_{82} assembling into close-packed island with almost uniform orientation (Figure 4b). Considering the commensurability between the center-to-center distance of Gd@C_{82} and the lattice of the underlying Cu(111), the intermolecular alignment is rationalized as ($\sqrt{19} \times \sqrt{19}$) R23.4°/Cu(111) as labeled by a black parallelogram. By recalling STM-derived intramolecular striped features along with STM simulations of Gd@C_{82} with R1 and R2 configuration, and analyzing molecular orientation population over 30 Gd@C_{82} assemblies, we find Gd@C_{82} adopting R1 orientation, in analogy with the energetically favorable configuration of isolated one, is abundant. It seems that Gd@C_{82} is inclined to rotate from "lying-down" configuration (R2) to tilting adsorption configuration (R1) during annealing at 850 K. Sufficient thermal activation at 850 K induces the assembled Gd@C_{82} fullerenes resembling the same interfacial binding geometry as that of isolated ones, indicative of the feasibility of two-dimensionally integrating single-Gd@C_{82} based moletronic device with performances almost unchanged.

In general, the assembly of molecules on surfaces depends on the balance between the in-plane intermolecular interaction and the molecule−substrate interaction.[33] While assembling into an island, the absence of the second Gd@C_{82} layer implies the relatively stronger Gd@C_{82}−Cu(111) interaction. We further quantitatively analyze the interaction strength at DFT calculation levels and find that the Gd@C_{82}−Cu(111) interaction is 0.13 eV stronger than the inter-Gd@C_{82} interaction. Moreover, it was found that the interaction between metallofullerenes, especially the dipole−dipole interaction, for example, induced three predominant orientations of Dy@C_{82} within the assembled island on Au(111),[34] and gave rise to the head-to-tail alignment of Nd@C_{82}.[35] At mild temperatures, the underlying copper atoms are not uniformly reconstructed by Gd@C_{82}, resulting in essentially different Gd@C_{82}/Cu(111) bonding geometry and orientations. This weakens the in-plane inter-Gd@C_{82} interaction, especially the dipole−dipole interaction, so Gd@C_{82} adopts random orientation. Upon annealing at 850 K, Gd@C_{82} uniformly reconstructs the underlying Cu(111), and the assembled Gd@C_{82} fullerenes sink into the substrate by one-copper-layer-deep,[19] with almost uniform Gd@C_{82}/Cu(111) interfacial character. The in-plane interaction between Gd@C_{82}, enhanced by the dipole−dipole interaction, makes Gd@C_{82} prefer adopting uniform orientational configuration. Recently, studies on the interfacial system constructed by copper and C_{60} reveal that spin-ordered states localize at the interface reconstruction and electron transfer induces magnetic hardening of the interfacial copper atoms,[36] which demonstrates the possibility of making diamagnetic copper ferromagnetic through controlling charge transfer at a copper−fullerene interface via exploitation of molecular coupling, for example, uniformly engineering the interface between Gd@C_{82} and Cu(111) here.

A straightforward comparison of the electronic states of assembled Gd@C_{82} with that of an individual one provides a comprehensive picture about the influence mechanism of the in-plane inter-Gd@C_{82} interaction on the electronic features, which would be helpful for qualitatively addressing the origin of the STS states. For precise comparison, we choose Gd@C_{82} with R1 orientation, for example, the one labeled by an arrow, and probe the dI/dV spectrum at its center. As shown in Figure 4c, it is revealed that STS states **B**, **C**, and **D** have energy downshift of about 0.06, 0.16, and 0.11 eV, respectively. It is reasonable that states **B** and **C** are the C_{82} cage/Cu(111) hybrid states with higher C_{82} cage contribution and readily modified by the dipole−dipole interfulleren interaction. Furthermore, the energy shifting of state **D** also verifies the Gd/cage hybrid state with majority contribution from C_{82} cage. Note that energy state **A** remains unchanged, indicative of the cage/Cu(111) hybrid state with higher Cu(111) contribution, which further proves the essentially identical Gd@C_{82}/Cu(111) interfacial character as that of the individual one. Additionally, the energy position of states **E** and **F** for Gd@C_{82} also remains unchanged upon assembling, in line with the PDOS results that they belong to the Gd/cage hybrid states with major contribution of endohedral Gd.

■ CONCLUSION

The interfacial geometry, adsorption configuration, the nature of electronic hybrid states, in-plane intermolecular interaction assisted assembly and modified electronic states of metallofullerene Gd@C_{82} were systematically studied. Compelling evidence for the energetically favored tilting orientational configuration of isolated Gd@C_{82}, such as DFT calculation and STS mapping, were provided. We clarify that Gd@C_{82} fullerens prefer restoring the tilting orientational configuration by balancing the Gd@C_{82}−Cu(111) interaction and the inter-Gd@C_{82} interaction, especially the dipole−dipole interaction, upon assembling and sufficient thermal activation. This provides a useful guideline for high-level integration of single-Gd@C_{82} based moletronic device with performances almost unchanged. Moreover, by comparing the electronic hybrid states of assembled Gd@C_{82} with that of individual one, we provide new insight into the impact of the inter-Gd@C_{82} interaction on the electronic states, and qualitatively attribute the shown C_{82} cage/Cu(111) and Gd/cage hybrid states to Cu(111)-, C_{82} cage- and Gd-dominant hybrid states, respectively.

■ AUTHOR INFORMATION

Corresponding Author

* Tel.:+86 27 8719 8256; fax: +86 27 8719 8576; e-mail zhqin@wipm.ac.cn (Z.H.Q.).

DOI: 10.1021/acs.langmuir.5b02965
Langmuir 2015, 31, 11438−11442

Notes

The authors declare no competing financial interest.

■ ACKNOWLEDGMENTS

This work was financially supported by the National Key Basic Research Program of China (Grant No. 2013CBA01601). Also, we are grateful to Prof. H. -J. Gao at IOP, CAS, for fruitful discussions.

■ REFERENCES

(1) Yasutake, Y.; Shi, Z.; Okazaki, T.; Shinohara, H.; Majima, Y. Single Molecular Orientation Switching of an Endohedral Metallofullerene. *Nano Lett.* **2005**, *5*, 1057−1060.

(2) Okamura, N.; Yoshida, K.; Sakata, S.; Hirakawa, K. Electron Transport in Endohedral Metallofullerene Ce@C_{82} Single-molecule Transistors. *Appl. Phys. Lett.* **2015**, *106*, 043108.

(3) Shinohara, H. Endohedral Metallofullerenes. *Rep. Prog. Phys.* **2000**, *63*, 843−892.

(4) Lu, X.; Feng, L.; Akasaka, T.; Nagase, S. Current Status and Future Developments of Endohedral Metallofullerenes. *Chem. Soc. Rev.* **2012**, *41*, 7723−7760.

(5) Yan, L.; Zhao, F.; Li, S.; Hu, Z.; Zhao, Y. Low-toxic and Safe Nanomaterials by Surface-chemical Design, Carbon nanotubes, Fullerenes, Metallofullerenes, and Graphenes. *Nanoscale* **2011**, *3*, 362−382.

(6) Lee, J.; Kim, H.; Kahng, S. J.; Kim, G.; Son, Y. W.; Ihm, J.; Kato, H.; Wang, Z. W.; Okazaki, T.; Shinohara, H.; Kuk, Y. Bandgap Modulation of Carbon Nanotubes by Encapsulated Metallofullerenes. *Nature* **2002**, *415*, 1005−1008.

(7) Hirahara, K.; Suenaga, K.; Bandow, S.; Kato, H.; Okazaki, T.; Shinohara, H.; Iijima, S. One-Dimensional Metallofullerene Crystal Generated Inside Single-Walled Carbon Nanotubes. *Phys. Rev. Lett.* **2000**, *85*, 5384.

(8) Jiang, J.; Gao, B.; Hu, Z. P.; Lu, W.; Wu, Z. Y.; Yang, J. L.; Luo, Y. Identification of Metal-Cage Coupling in a Single Metallofullerene by Inelastic Electron Tunneling Spectroscopy. *Appl. Phys. Lett.* **2010**, *96*, 253110.

(9) Nishibori, E.; Iwata, K.; Sakata, M.; Takata, M.; Tanaka, H.; Kato, H.; Shinohara, H. Anomalous Endohedral Structure of Gd@C_{82} Metallofullerenes. *Phys. Rev. B: Condens. Matter Mater. Phys.* **2004**, *69*, 113412.

(10) Liu, L.; Gao, B.; Chu, W.; Chen, D.; Hu, T.; Wang, C.; Dunsch, L.; Marcelli, A.; Luo, Y.; Wu, Z. The Structural Determination of Endohedral Metallofullerene Gd@C_{82} by XANES. *Chem. Commun.* **2008**, *4*, 474−476.

(11) Senapati, L.; Schrier, J.; Whaley, K. B. Electronic Transport, Structure, and Energetics of Endohedral Gd@C_{82} Metallofullerenes. *Nano Lett.* **2004**, *4*, 2073−2078.

(12) Wang, L.; Yang, D. Comment on "Electronic Transport, Structure, and Energetics of Endohedral Gd@C_{82} Metallofullerenes. *Nano Lett.* **2005**, *5*, 2340.

(13) Senapati, L.; Schrier, J.; Whaley, K. B. Reply to Comment on "Electronic Transport, Structure, and Energetics of Endohedral Gd@C_{82} Metallofullerenes. *Nano Lett.* **2005**, *5*, 2341.

(14) Mizorogi, N.; Nagase, S. Do Eu@C_{82} and Gd@C_{82} Have an Anomalous Endohedral Structure? *Chem. Phys. Lett.* **2006**, *431*, 110−112.

(15) Sebetci, A.; Richter, M. Gd@C_{82}: Origin of the Antiferromagnetic Coupling between Endohedral Gd and the Free Spin on the Carbon Cage. *J. Phys. Chem. C* **2010**, *114*, 15−19.

(16) Suzuki, M.; Lu, X.; Sato, S.; Nikawa, H.; Mizorogi, N.; Slanina, Z.; Tsuchiya, T.; Nagase, S.; Akasaka, T. Where Does the Metal Cation Stay in Gd@C_{2v}(9)-C_{82}? A Single-Crystal X-ray Diffraction Study. *Inorg. Chem.* **2012**, *51*, 5270−5273.

(17) Dai, X.; Gao, Y.; Xin, M.; Wang, Z.; Zhou, R. The Ground State and Electronic Structure of Gd@C_{82}: A Systematic Theoretical Investigation of First Principle Density Functionals. *J. Chem. Phys.* **2014**, *141*, 244306.

(18) Grobis, M.; Khoo, K. H.; Yamachika, R.; Lu, X.; Nagaoka, K.; Louie, S.; Crommie, M. F.; Kato, H.; Shinohara, H. Spatially Dependent Inelastic Tunneling in a Single Metallofullerene. *Phys. Rev. Lett.* **2005**, *94*, 136802.

(19) Chen, J.; Qin, Z. H.; Pan, J.; Lu, S.; Du, S. X.; Gao, H.-J.; Cao, G. Y. Scanning Tunneling Microscopy Study of Molecular Growth Structures of Gd@C_{82} on Cu(111). *Chin. Phys. B* **2013**, *22*, 076802.

(20) Zhao, S.; Zhang, J.; Dong, J.; Yuan, B.; Qiu, X.; Yang, S.; Hao, J.; Zhang, H.; Yuan, H.; Xing, G.; Zhao, Y.; Sun, B. Scanning Tunneling Microscopy Investigation of Substrate-Dependent Adsorption and Assembly of Metallofullerene Gd@C_{82} on Cu(111) and Cu(100). *J. Phys. Chem. C* **2011**, *115*, 6265−6268.

(21) Zhang, J.; Zhao, S. X.; Yuan, B. K.; Deng, K.; Sun, B. Y.; Qiu, X. H. Monolayered Adatom Aggregation Induced by Metallofullerene Molecules on Cu(100). *Surf. Sci.* **2012**, *606*, 78−82.

(22) Funasaka, H.; Sakurai, K.; Oda, Y.; Yamamoto, K.; Takahashi, T. Magnetic Properties of Gd@C_{82} Metallofullerene. *Chem. Phys. Lett.* **1995**, *232*, 273−277.

(23) Horcas, I.; Fernández, R.; Gómez-Rodríguez, J. M.; Colchero, J.; Gómez-Herrero, J.; Baro, A. M. WSXM: A Software for Scanning Probe Microscopy and a Tool for Nanotechnology. *Rev. Sci. Instrum.* **2007**, *78*, 013705.

(24) Kresse, G.; Furthmüller, J. Efficient Iterative Schemes for Ab Initio Total-Energy Calculations Using a Plane-Wave Basis Set. *Phys. Rev. B: Condens. Matter Mater. Phys.* **1996**, *54*, 11169−11186.

(25) Perdew, J. P.; Burke, K.; Ernzerhof, M. Generalized Gradient Approximation Made Simple. *Phys. Rev. Lett.* **1996**, *77*, 3865−3868.

(26) Blöchl, P. E. Projector augmented-wave method. *Phys. Rev. B: Condens. Matter Mater. Phys.* **1994**, *50*, 17953−17979.

(27) Lee, K.; Murray, É. D.; Kong, L.; Lundqvist, B. I.; Langreth, D. C. Higher-Accuracy van der Waals Density Functional. *Phys. Rev. B: Condens. Matter Mater. Phys.* **2010**, *82*, 081101.

(28) Smoluchowski, R. Anisotropy of the Electronic Work Function of Metals. *Phys. Rev.* **1941**, *60*, 661−674.

(29) Hasegawa, Y.; Ling, Y.; Yamazaki, S.; Hashizume, T.; Shinohara, H.; Sakai, A.; Pickering, H. W.; Sakurai, T. STM Study of One-dimensional Cluster Formation of Fullerenes: Dimerization of Y@C_{82}. *Phys. Rev. B: Condens. Matter Mater. Phys.* **1997**, *56*, 6470.

(30) Miyazaki, T.; Sumii, R.; Umemoto, H.; Okimoto, H.; Ito, Y.; Sugai, T.; Shinohara, H.; Zaima, T.; Yagi, H.; Hino, S. Ultraviolet Photoelectron Spectra of Er_2@C_{82}(I), Er_2@C_{82}(III), Er_2C_2@C_{82}(I) and Er_2C_2@C_{82}(III). *Chem. Phys.* **2012**, *397*, 87−91.

(31) Muthukumar, K.; Stróżecka, A.; Mysliveček, J.; Dybek, A.; Dennis, T. J. S.; Voigtländer, B.; Larsson, J. A. Endohedral Fullerene Ce@C_{82} on Cu(111): Orientation, Electronic Structure, and Electron-Vibration Coupling. *J. Phys. Chem. C* **2013**, *117*, 1656−1662.

(32) Wang, K.; Zhao, J.; Yang, S.; Chen, L.; Li, Q.; Wang, B.; Yang, S.; Yang, J.; Hou, J. G.; Zhu, Q. Unveiling Metal-Cage Hybrid States in a Single Endohedral Metallofullerene. *Phys. Rev. Lett.* **2003**, *91*, 185504.

(33) Qin, Z. H. Controllable Growth of Low-dimensional Nanostructures on Well-defined Surfaces. *Chin. Phys. B* **2013**, *22*, 098108.

(34) Chen, F.-Y.; Hu, Z.-P. Coverage-dependent Orientations of Dy@C_{82} Molecules on Au(111) Surface. *Chin. J. Chem. Phys.* **2012**, *25*, 423−428.

(35) Lin, N.; Huang, H.; Yang, S.; Cue, N. Nucleation of Endohedral Metallofullerene Nd@C_{82} on C_{60} Films. *Phys. Rev. B: Condens. Matter Mater. Phys.* **1998**, *58*, 2126−2130.

(36) Al Ma'Mari, F.; Moorsom, T.; Teobaldi, G.; Deacon, W.; Prokscha, T.; Luetkens, H.; Lee, S.; Sterbinsky, G. E.; Arena, D. A.; MacLaren, D. A.; Flokstra, M.; Ali, M.; Wheeler, M. C.; Burnell, G.; Hickey, B. J.; Cespedes, O. Beating the Stoner Criterion Using Molecular Interfaces. *Nature* **2015**, *524*, 69−73.

DOI: 10.1021/acs.langmuir.5b02965
Langmuir 2015, 31, 11438−11442